

# High Performance Electric Double-layer Capacitors Using Mass Produced Multi-walled Carbon Nanotubes

Morinobu Endo<sup>1\*</sup>, Yong Jung Kim<sup>1</sup>, Teruaki Chino<sup>1</sup>, Ozaki Shinya<sup>1</sup>, Yutaka Matsuzawa<sup>1</sup>,

Hiroaki Suezaki<sup>1</sup>, Kriengkamol Tantrakarn<sup>1</sup>, Mildred S. Dresselhaus<sup>2</sup>

<sup>1</sup> Faculty of Engineering, Shinshu University, 4-17-1 Wakasato, Nagano 380-8553, Japan

<sup>2</sup> Department of Physics and Department of Electrical Engineering, and Computer Science, MIT,  
Cambridge, Massachusetts 02139, USA

\* corresponding author; M. Endo

E-mail; [endo@endomoribu.shinshu-u.ac.jp](mailto:endo@endomoribu.shinshu-u.ac.jp)

Tel; +81-26-269-5201, Fax; +81-26-269-5208

## Abstract

Mass-produced multi-walled carbon nanotubes (MWNTs, which has the trademark of VGNF<sup>®</sup>) has been investigated for their potential for use in electric double layer capacitors (EDLCs). The variation aspects of this MWNT by KOH activation showed quite interesting features. The gravimetric capacitance enhancement and specific surface area (SSA) on KOH activation increased linearly. However, the capacitance per unit surface area has a maximum at 200 wt. % of KOH addition. After all, the VGNF-KOH 500 sample exhibits a capacitance enhancement as much as 13 times greater ( $28.3 \text{ F g}^{-1}$ ) than that of the as-grown materials ( $2.2 \text{ F g}^{-1}$ ).

$\text{g}^{-1}$ ), under the conditions of charging up to 3.5V and discharging at a current density of  $10\text{mA}/\text{cm}^2$ . Interestingly, for this MWNT (VGNF<sup>®</sup>), selective attack on its amorphous carbon impurity has also been observed, as demonstrated from both SEM observations and Raman spectra. Consequently, the results of this study will provide insight into the potentiality of using MWNTs for EDLC electrodes, which would enable the cheapest production cost among the various types of carbon nanotubes.

## 1. Introduction

Much work has been done over the past decades, both on the fundamental side and on the technological development of materials with high performance for use in electric double-layer capacitor (EDLC) electrodes. In the development of EDLCs, it is very important to note that these materials, which are used as an electrode, significantly contribute to increase the performances of EDLCs. Amongst the various carbon candidate materials for use in EDLC electrodes, carbon nanotubes (CNTs) have been proposed as being especially attractive [1-5], due to : (1) the useful space within their cores and between neighboring tubes and (2) a good accessibility of these surfaces. In 1997, Niu et al. first suggested [1] that CNTs could be used in electrochemical capacitors (supercapacitors and/or ultracapacitors), using catalytically grown carbon nanotubes, 0.8 nm in diameter, commercially produced by Hyperion Catalysis International (Graphite fibrils <sup>TM</sup>). They have focused on the high surface area availability, low resistivity, and high stability of CNTs. With these CNTs, they were able to obtain a gravimetric capacitance of 102 F/g at 1 Hz on a single cell device, employing 38 wt. % sulfuric acid in an aqueous electrolyte. Two years later, Liu et al. [2] reported an excellent result of 283 F/g using single-wall carbon nanotubes (SWNTs) with a nonaqueous electrolyte (0.1 M TBAPF<sub>6</sub>/acetonitrile) with a conventional three-compartment system. The calculation method of the capacitance measurement involved using a cyclic-voltammogram at a scan rate of 50 mV/s.

Attempts to produce EDLC electrode materials based on CNTs can be divided into three nanotube categories: 1) SWNTs [2, 5-8], 2) MWNTs [1, 3, 4] and 3) modified CNTs with activation [9], and coating the nanotube with a conducting polymer, such as *poly*(pyrrole) [10, 11], *poly*(aniline) [12, 13] and *poly*(thiophene) [14].

With respect to mass production, the high cost for manufacturing of CNTs is considered as a problematic drawback for practical applications. Thus, the capacitance behavior has been examined for such a MWNT (VGNF<sup>®</sup>) which has been manufactured by mass production methods and already is on the market. Mass production will inevitably reduce production costs. Unfortunately, it is not easy to apply the VGNF<sup>®</sup> to EDLC electrodes directly to EDLCs systems, since they have quite a small specific surface area (SSA) (ca. 20 m<sup>2</sup>/g). Therefore, we tried to use activation in order to obtain a sufficient specific surface area by using a chemical reagent (KOH). Furthermore, the diameter of these fibers could be controlled by the amount of catalyst added (ferrocene) during the synthesis. VGNF<sup>®</sup> has an average diameter about half (ca. 80 nm) that of VGCF<sup>®</sup> which is the one trademark of SDK.

In this work, we show the structural variations as a function of KOH addition of the mass-produced MWNTs with smaller size in diameter. Consequently, it could be confirmed that the structural variations are correlated with the capacitance uptake of each sample.

## 2. Experimental

### *2.1 Description of the manufacturing process of VGNF and their activation with KOH*

Recently, SDK have developed a MWNT (VGNF<sup>®</sup>) with an average cross-sectional diameter of 80nm. On the completion of 10 ton/yrs mass production capability, SDK will now step up its effort to develop the mass production of VGNF<sup>®</sup> which is a trademark of Showa Denko K. K. (SDK). In this study, this mass produced multi-walled carbon nanotube (MWNT), is used as an active material for EDLCs. This MWNT is prepared by mass production using a floating reactant method [15, 16]. The mass production inevitably reduces the production costs. Furthermore, the diameter of these fibers can be controlled by the amount of catalyst added (ferrocene) during the synthesis. In order to obtain a sufficient specific surface area, an activation process was added using a chemical reagent (KOH). The activation was carried out at a fixed rate (5 /min) in a argon flow (200 ml/min), and each sample was maintained for 1 h at 800 . After activation, the sample was cooled in an inert atmosphere. The samples obtained were washed with deionized water to eliminate the remaining KOH, and, finally, they were dried at room temperature. The mixing ratio was varied from 1 to 5 (=KOH/VGNF<sup>®</sup>). The samples were designated by the amount of KOH addition for the activation process, e.g., VGNF-KOH 100 is the sample activated with 100wt. % of KOH using VGNF<sup>®</sup> as a host carbon material.

## *2.2 Characterization*

The nitrogen adsorption isotherms were measured at liquid-nitrogen temperature using an ASAP 2010 instrument (Micromeritics, USA). The specific surface area was determined using the multi-point Brunauer-Emmett-Teller (BET) method. Moreover, the pore volume, pore diameter, and pore size distribution were obtained using a variety of other methods. Raman spectra were taken at room temperature under ambient conditions using a Kaiser optical system (RamanRXN system, USA). The excitation source was a 514.5nm Ar-ion laser and the optical power at the sample position was maintained below 5 mW. The spectra were averaged over three scans to improve the signal-to-noise ratio, and the data were corrected for the spectral response of the instrument. The R values (relative intensity of the D to G peaks,  $I_D/I_G$ ) were calculated from five measurements by ignoring the maximum and minimum values to reduce the deviations due to the different areas on the samples. Transmission electron microscope observations (HRTEM, JEM2010FEF, JEOL Co, Ltd., Japan, 200kV) were performed to confirm the detailed modification of the fiber surface. Field-emission scanning electron microscopy (FE-SEM, JEOL JSM-6335F, Japan, 10kV) images were used to confirm the morphological variations.

### ***2.3 Capacitance measurement***

In the electrochemical experiments, a two-terminal system was used with no reference electrode, because almost all commercially packaged electrical capacitor devices have two-terminal systems with a symmetric configuration. Under this condition, of course, an overall evaluation of the two-electrode system is obtained, so that information on the behavior of each electrode interface is not available from such measurements. However, in practice, useful performance information regarding the charging and discharging capacity, the energy density and the power density of capacitor devices are easily obtained by means of two-terminal measurements [17]. Sheet type electrodes around 0.4 mm thick were made using 5wt% poly-tetrafluoroethylene (PTFE) as a binder, and a glassy-carbon plate was used as a current collector. The test cell was fabricated using two of the electrodes face to face, with a separator inserted between them. 1M of tetraethylammonium tetrafluoroborate (TEABF<sub>4</sub>) was used as an electrolyte in an organic solvent (propylene carbonate, PC). Charge and discharge cycles were performed at constant current, and the capacitance was obtained from the current density variation of the discharge (1~60mA/cm<sup>2</sup>). The ESR (equivalent series resistance) was measured at 1 kHz with an alternating current.

### **3. Results and discussion**

In order to clarify the difference in diameter, the other mass-produced MWNT (VGCF<sup>®</sup>), prepared by the same method has been compared by means of electron microscopy. Figure 1 shows the overall morphology of as-grown VGCF<sup>®</sup> and VGNF<sup>®</sup> obtained using FE-SEM (a, b, respectively) and the highly magnified structure on an individual fiber using HR-TEM (c, d). As observed in figure 1, the VGCF (150nm in average diameter) has much larger value than that of VGNF (80nm in average diameter) in diameter. In this figure, it is the difference in diameter that purposed to clarify between the both multi-walled carbon nanotubes, although the values obtained by TEM photographs showed *ca.* 30nm on VGCF and *ca.* 20nm on VGNF. Because the TEM observation is limited in very small area, it is not representative entirely of samples. Therefore, the data supplied from the manufacturer were shown here. Figures 1 (a, b) were taken at a magnification of 10,000 times with 5kV of acceleration voltage. Regarding the SEM observation, distinctive differences in morphology were readily confirmed. VGNF<sup>®</sup> has a relatively smaller diameter than that of VGCF and it contains many impurities, such as amorphous particles etc. Such a morphological difference is attributed to the growth kinetics of the synthesis process, which depends on the amount of catalyst employed. The differences on growth kinetics imply the probability of making contact among the catalyst particles and the feedstock to produce a carbon skeleton. In the floating reactant method, the growth mechanism of the fibers has been ascertained as consisting of two steps, one of formation and the other of



thickening [18]. The formation of fibers is initiated when the feedstock contacts the catalyst through mass transfer. For a small feeding content of catalyst, the possibility of such a contact is inevitably reduced. Therefore, before the thickening process consumes the feedstock or is self-assembled, amorphous particles are formed. It is well known that the VGCFs have a central tube [19] and that carbon nanotubes (CNTs) were reported by Ijima [20]. From HR-TEM observations, the studied MWNTs exhibit a pleated graphene layer, which is considered to be a turbostratic structure, in the longitudinal direction with a wide hollow canal. This demonstrates that the fine structure between them is very similar, but different in diameter. Because the smaller diameter can contribute to the higher specific surface area, we focused in this paper on the smaller MWNT with the brand name of VGNF.

Figure 2 shows the nitrogen adsorption-desorption isotherms of MWNTs activated at 800 °C by using KOH/MWNT ratios of 1 to 5 (weight %), where the blank symbols indicate the adsorption results and the gray symbols imply results from the desorption. In figure 2, the open symbols indicate the results obtained from the pristine as-grown fibers, and the filled symbols indicate the results for the MWNTs activated with KOH addition in the range of 100 to 500 wt. %. From the results, the amount of adsorbed nitrogen continuously increased as the KOH increased. In contrast to the intact as-grown MWNTs which show no hysteresis loops, hysteresis loops can be observed in all samples activated with KOH, which is associated with capillary condensation occurring in

the mesopores. Moreover, the  $N_2$  adsorption at a low relative pressure ( $<0.1 P/P_0$ ) also gradually increases as a function of KOH addition, which resulted in a change from type IV to type II behavior. The development of micropores becomes prominent at a large KOH addition (more than 400 wt. %).

In Figure 3, the mesopore size distributions calculated from desorption profiles, using the BJH (Barrett-Joyner-Halenda) method have demonstrated that the particular pore sizes of 4 nm in diameter continuously increased as the KOH addition increased. While there was no sharp peak based on adsorption isotherms, it was found that the very sharp peaks at 4 nm were induced by KOH activation. It can be imagined that this is due to the nitrogen molecules that are either introducing or leaving between the ordered graphene layers, which result in difference of surface tension between the adsorption and the desorption. Of course, it is not clear whether the adsorption or the desorption data should be considered to calculate the pore size. Some references have suggested adopting the desorption data as being more preferable for obtaining the pore size distributions, because the desorption process is more thermodynamically stable than the adsorption process.

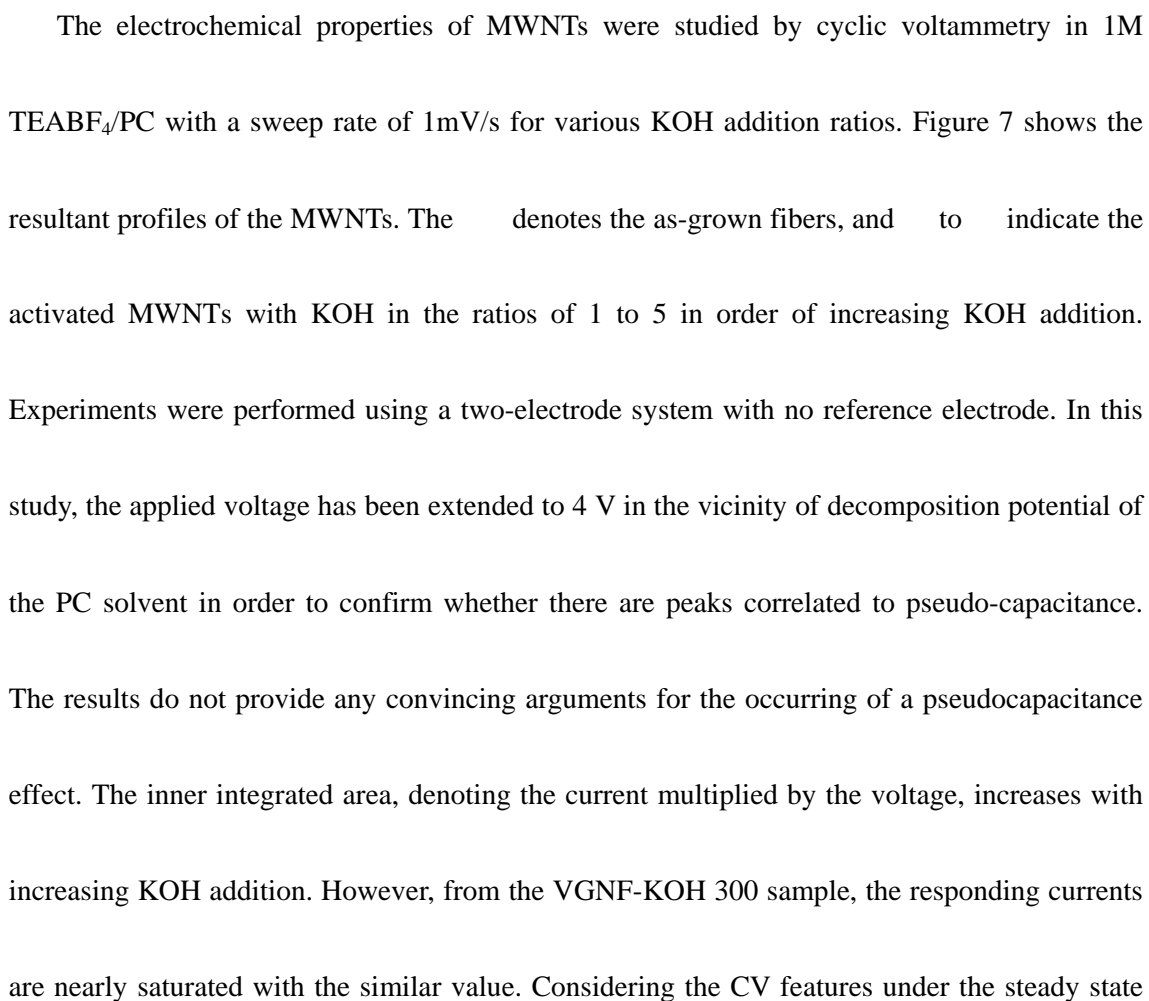
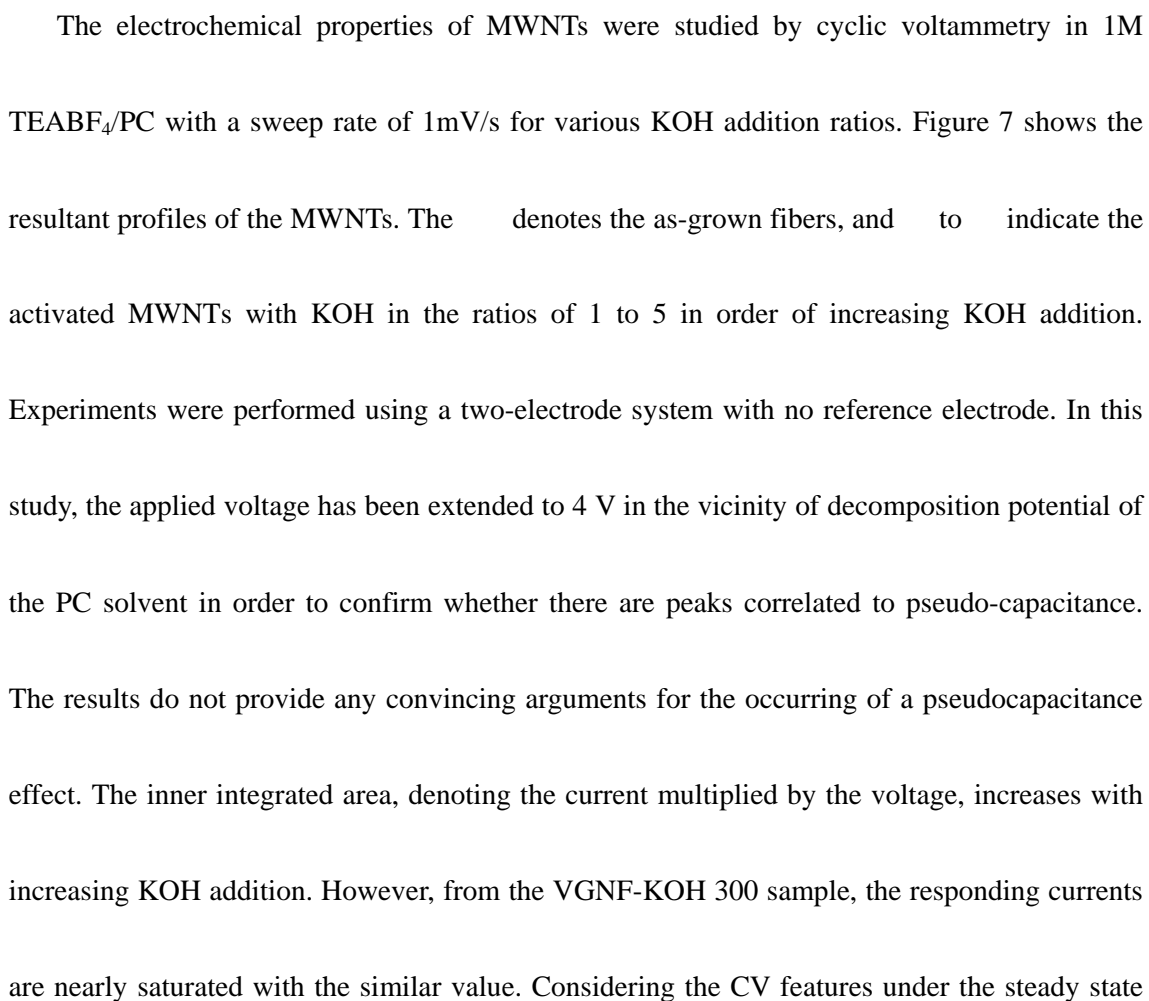
The fundamental BET properties of the MWNTs as a function of KOH addition are summarized and compared in Table 1. As can be seen, KOH addition is quite effective to improve the specific surface area (SSA). The resulting SSA at 500 wt. % of KOH addition is as

much as 12 times greater than that of as-grown MWNTs. The total pore volume increased up to 400 wt. % of KOH addition from  $0.11$  to  $0.44 \text{ cm}^3 \text{ g}^{-1}$ , but for the case of 500 wt. % of addition the data show some deviation which decreased to  $0.37 \text{ cm}^3 \text{ g}^{-1}$ . All samples are dominated by mesoporous structure.

Figure 4 shows morphological variations of MWNTs after KOH activation using FE-SEM (a-c) and HR-TEM (d-f). Figure 4 (a-c) represents the MWNTs activated with KOH at (a) 100 wt. %, (b) 300 wt. % and (c) 500 wt. %. TEM photographs from (d) to (f) also taken in the same order. All photographs were taken at a magnification of  $10,000 \times$  on SEM and  $250,000 \times$  on TEM. In contrast that the herringbone type fibers [21] and MWNT prepared by hydrocarbon decomposition of acetylene on cobalt supported on silica [22], MWNTs used in this study maintain their fibrous morphology even through the addition of 500 wt. % of KOH. Notice that significant amounts of the impurity carbons that are present in the as-grown MWNTs have been consumed after KOH activation. This phenomenon has also been reported by Beguin et al. [23] using NaOH as a chemical agent for activation. The fine structure of the fiber surface is also illustrated, namely that the diverse defects on MWNTs gradually increase with increasing KOH addition. The VGNF-KOH 500 shows relatively large defects, and drastically narrowed fiber diameters along the cross-sectional direction were confirmed. The defects present on the carbon skeleton structure contribute to the variations seen in the Raman spectra.

In Figure 5, room temperature Raman spectra of chemically activated MWNTS are shown. Two conventional G ( $\sim 1580\text{cm}^{-1}$ ) and D ( $\sim 1360\text{cm}^{-1}$ ) peaks appear in the first-order spectra. Thus, the vibrational characteristics of carbonaceous materials exhibited in these Raman spectra allow distinct features to be identified [24, 25]. Using a Lorentzian fit to these data, the relative ratio (R) of the integrated intensities for the D and G lines and the lateral extent of the graphene layers have been calculated [26]. The results are shown in Fig. 6. Figures 6 (a) and (b) show the relative intensity variations of the Raman lines (R) and the lateral crystallite size of the MWNTs as a function of KOH addition. In order to reduce the deviations introduced, R values were obtained from the average of the five measurements, by ignoring the maximum and minimum values. Interestingly, after KOH activation, MWNTs show a drastic reduction in the R value. Although the variation of R as a function of the KOH addition is gradual (0.87 and 0.83 on the 100 and 500 wt. % of KOH addition, respectively), the large differences between the as-grown and the activated MWMT is clearly confirmed (1.03 and 0.87 on the as-grown and 100 wt. % of KOH addition, respectively). This interesting phenomenon is ascribed to the preferential attack of KOH on the amorphous carbon structures that exists abundantly on as-grown MWNTs, as demonstrated in the SEM observation in Figure 4. Differences between the as-grown and KOH-activated samples in the first-order Raman spectra are hardly distinguishable. On the other hand, the result from the 200 wt. % addition of KOH starts to show a shoulder on the G peak

due to the  $D'$  peak at  $1620\text{ cm}^{-1}$ , which is attributed to structural defects [27]. Consideration of the second-order Raman spectra provides greater clarity as to the structural morphology, showing three distinctive peaks at  $\sim 2720$ ,  $\sim 2962$ ,  $\sim 3246\text{ cm}^{-1}$ , indicating the  $G'$  (D overtone),  $D'$  band (combination of D and G bands) and the  $D'$  overtone, respectively. The  $G'$  peak and  $D'$  overtone obtained from the activated MWNTs has a sharper and distinctive shape, which implies that the second-order spectra clearly demonstrate the selective attack on amorphous carbon by KOH.

The electrochemical properties of MWNTs were studied by cyclic voltammetry in 1M TEABF<sub>4</sub>/PC with a sweep rate of 1mV/s for various KOH addition ratios. Figure 7 shows the resultant profiles of the MWNTs. The  denotes the as-grown fibers, and  to indicate the activated MWNTs with KOH in the ratios of 1 to 5 in order of increasing KOH addition. Experiments were performed using a two-electrode system with no reference electrode. In this study, the applied voltage has been extended to 4 V in the vicinity of decomposition potential of the PC solvent in order to confirm whether there are peaks correlated to pseudo-capacitance. The results do not provide any convincing arguments for the occurring of a pseudocapacitance effect. The inner integrated area, denoting the current multiplied by the voltage, increases with increasing KOH addition. However, from the VGNF-KOH 300 sample, the responding currents are nearly saturated with the similar value. Considering the CV features under the steady state

below 3V, the CV profiles show features near an ideal rectangular shape.

Figure 8 indicates the variations in the specific capacitance per unit weight (F/g) obtained from the KOH-activated MWNTs. In order to consider the effect of the applied potential for a charge and current density during discharge, the resultant capacitances are identified by their charged voltage; (a) capacitance uptake when MWNTs are charged to 2.5 V, and (b) to 3.5 V. In this figure, open symbols are used for data obtained at  $1\text{mA/cm}^2$  of current density on discharge and gray symbols refer to a  $10\text{mA/cm}^2$ . As for MWNTs charged to 2.5V (Figure 8(a)), MWNTs show a nearly linear increase in the gravimetric capacitance (F/g) as the KOH addition is increased. The final resulting capacitance of the VGNF-KOH 500 (*ca.* 14 F/g) shows an enhancement on the capacitance uptake compared to that of the as-grown fiber (*ca.* 2 F/g). Furthermore, the effect of the discharge current density on the capacitance uptake is nearly negligible as for charged up to 2.5V. Considering the charge behavior up to 3.5V (Figure 8 (b)), the overall features of the capacitance uptake curves are quite different. Initially, the increasing rates of capacitances are increased by a factor of 3 to 4 at  $1\text{ mA/cm}^2$  and  $10\text{ mA/cm}^2$ , respectively. The increasing features are also changed from linear to concave behavior as a function of KOH addition. Secondly, the effect of the current density on capacitance uptake is somewhat enhanced. **The higher the current density that is applied on discharge, the higher the capacitance that is obtained.** The enhancement of the capacitance uptake by using a higher

charging voltage can be attributed to micropores created by the KOH activation. i.e., ions dispersed in the solvent are forced into the pores, thus contributing to increasing the capacitance.

Figure 9 represents the variation of the specific capacitance per unit area ( $\mu\text{F}/\text{cm}^2$ ) as a function of KOH addition for both series of samples. The symbols used here are the same as those in Figure 8. The capacitances per unit surface area that are permitted here allow comparing our results with the results from references [28], and the specific capacitance implies the ion accessibility into the porous structure [29]. The specific capacitance per unit area is preferred for the evaluation of the validity of the effect of the surface area on the capacitance uptake. To compare the results obtained from a conventional three-compartment system, the values shown here must be multiplied by 4, because all the present measurements were carried out under a symmetric two-electrode system [30]. As for the 2.5V charge data (Figure 10(a)), the effect of the current density is negligible, except for the case of as-grown fibers. The MWNTs show small decrease in their capacitances per unit area after the activation with KOH, and they exhibit almost the same values, lying in the range 4.5-7.7  $\mu\text{F}/\text{cm}^2$ . However, the behavior is changed in the results shown for 3.5V. Firstly, all the values are significantly enhanced by factors around 4 on the maximum and about 1.5 times on minimum (as-grown). Next, the effect of the current density features prominently in their capacitance uptake, which

has a difference of about  $2\mu\text{F}/\text{cm}^2$  over the overall range. In the as-grown samples, the capacitance decreased with increasing current density. Finally, the maximum capacitance is obtained after the activation. The capacitance based on unit area exhibits a maximum of  $19\mu\text{F}/\text{cm}^2$  (which is equivalent to  $76\mu\text{F}/\text{cm}^2$ . Such a high value can be attributed to the edge exposure of the graphitic lattice as demonstrated from the Raman spectra.) at a 200wt. % KOH addition. As was mentioned in Figure 8, these enhancements in the capacitance uptake at higher charging voltage are attributed to the micropores created by KOH activation. Furthermore, good accessibility to these surfaces on MWNTs and the edge exposure induced by KOH attack greatly contribute to such a high specific capacitance per unit area.

#### **4. Conclusion**

This study has investigated the structural variations resulting from KOH activation of MWNTs manufactured by a mass production process and their capacitance behavior has been examined using an organic solvent of 1M TEABF<sub>4</sub>/PC. Activation with KOH greatly enhanced their pore creation over the whole range of KOH addition. At higher KOH additions, an increase in the amounts of micropores was prominent. From the Raman spectra and SEM observations, interesting phenomena have been confirmed that the preferential elimination of the amorphous carbon impurity has been demonstrated. However, when over 200 wt. % of KOH is added for



activation, it is assumed that the excessive KOH attacks the surface of the carbon nanotubes (MWNTs) directly, corresponding to the appearance of the D' peak at  $1620\text{ cm}^{-1}$ . Furthermore, these structural variations are correlated with the resultant capacitance, based on unit weight and unit area. From the capacitance examination, KOH activation is found to be very useful to obtain a high capacitance uptake per unit weight. The effect of the charging voltage was examined also. The higher capacitance obtained by charging up to 3.5V relative to 2.5 V is attributed to a chemical reaction due to the decomposition of the electrolyte on the carbon host material as the electrode and ions are forced into the narrow pores. The capacitance per unit area confirmed this explanation. i.e., when charging to 2.5 V, the activated samples have a lower value than that of the as-grown material. On the basis of these diverse investigations, the characteristic properties of mass-produced MWNTs, activated with KOH have been studied and the potential of these materials for EDLC device applications have been confirmed.

### **Acknowledgements**

This work was partially supported by the CLUSTER of Ministry of Education, Culture, Sports, Science and Technology.

### **5. References**

1. Niu C, Sichel EK, Hoch R, Moy D, and Tennent H. High power electrochemical capacitors

based on carbon nanotube electrodes. *Appl. Phys. Lett.* 1997; 70: 1480-2

2. Liu CY, Bard AJ, Wudl F, Weitz I, and Heath JR. Electrochemical characterization of films of single-walled carbon nanotubes and their possible application in supercapacitors. *Electrochemical and Solid-State Letters* 1999; 2: 577-8.

3. Ma RZ, Liang J, Wei BQ, Zhang B, Xu CL, Wu DH. J. Study of electrochemical capacitors utilizing carbon nanotube electrodes. *J Power Sources* 1999; 84: 126-129

4. Frackowiak E, Metenier K, Bertagna V, and Beguin F. Supercapacitor electrodes from multiwalled carbon nanotubes. *Appl. Phys. Lett.* 2000; 77: 2421-3

5. An KH, Kim WS, Park YS, Choi YC, Lee SM, Chung DC, Bae DJ, Lim SC. Supercapacitor using single-walled carbon nanotube electrodes. *Adv. Mater.* 2001; 13: 497-500

6. Pico F, Rojo JM, Sanjuan ML, Anson A, Benito AM, Callejas MA, Maser WK, and Martinez MT. Single-walled carbon nanotubes as electrodes in supercapacitors. *J Electrochem. Soc.* 2004; 151: A831-7

7. Lee JY, An KH, Heo JK, Lee YH. Fabrication of supercapacitor electrodes using fluorinated single-walled carbon nanotubes. *J Phys. Chem. B* 2003; 107: 8812-5

8. Shiraishi S, Kurihara H, Okabae K, Hulicova D, Oya A. Electric double layer capacitance of highly pure single-walled carbon nanotubes (HiPco<sup>TM</sup> Buckytubes<sup>TM</sup>) in propylene carbonate electrolytes. *Electrochem. Comm.* 2002; 4: 593-8

9. Frackowiak E, Delpoux S, Jurewicz K, Szostak K, Cazorla-Amoros D, Beguin F. Enhanced capacitance of carbon nanotubes through chemical activation. *Chem. Phys. Lett.* 2002; 361: 35-41
10. Jurewicz K, Delpoux S, Bertagna V, Beguin F, Frackowiak E. Supercapacitors from nanotubes/polypyrrole composites. *Chem. Phys. Lett.* 2001; 347: 36-40
11. An KH, Jeon KK, Heo JK, Lim SC, Bae DJ, Lee YH. High-capacitance supercapacitor using a nanocomposite electrode of single-walled carbon nanotube and polypyrrole. *J Electrochem. Soc.* 2002; 149: A1058-62
12. Downs C, Nugent J, Ajayan PM, Duquette DJ and Santhanam KSV. Efficient polymerization of aniline at carbon nanotube electrodes. *Adv. Mater.* 1999; 11: 1028-31
13. Zhou YK, He BL, Zhou WJ, Huang J, Li XH, Wu B, Li HL. Electrochemical capacitance of well-coated single-walled carbon nanotube with polyaniline composites. *Electrochimica Acta* 2004; 49: 257-62.
14. Laforgue A, Simon P, Sarrazin C, Fauvarque JF. Polythiophene-based supercapacitors. *J Power Sources* 1999; 80: 142-8
15. Endo M. Growth carbon fibers in the vapor phase. *Chemtech* 1988; 18: 568-576.
16. Endo M, Kim YA, Hayashi T, Nishimura K, Matusita T, Miyashita K, Dresselhaus MS. Vapor-grown carbon fibers (VGCFs): Basic properties and their battery applications. *Carbon*

2001; 39: 1287-1297.

17. Conway BE. Electrochemical supercapacitors; scientific fundamentals and technological application. Kluwer Academic, Plenum publishers; New York: 1993.

18. Carbon nanotube; Preparation and properties, Ed. Thomas W. Ebbesen. NEC research Institute, Princeton, New Jersey, CRC press; Florida, USA: 1997.

19. Oberlin A, Endo M, Koyama T. Filamentous growth of carbon through benzene decomposition. J Crystal growth 1976; 32: 335-49

20. Ijima S. Helical microtubules of graphitic carbon. Nature 1991; **354**: 56-8

21. Yoon SH, Lim SY, Song Y, Ota Y, Qiao W, Tanaka A and Mochida I. KOH activation of carbon nanofibers. Carbon 2004; 42: 1723-9

22. Raymundo-Piñero E, Cazorla-Amorós D, Linares-Solano A, Delpeux S, Frackowiak E, Szostak K and Béguin F. High surface area carbon nanotubes prepared by chemical activation. Carbon 2002; 40, 1614-7.

23. Raymundo-Pinero E, Cacciaguerra T, Beguin F. A single step process for the simultaneous purification and opening of MWNTs, Extend abstracts, Carbon 2004, Providence, Rhode Island, USA: 2004

24. Ferrari AC and Robertson J. Interpretation of Raman spectra of disordered and amorphous carbon. Physical review B 2001; 61: 14095-107

25. Matthews MJ, Pimenta MA, Dresselhaus G, Dresselhaus MS, Endo M. Origin of dispersive effects of the Raman *D* band in carbon materials Physical review B 2001; 59: R6585-88
26. Knight DS, White WB. Characterization of diamond films by Raman spectroscopy. J Mater. Res. 1989; 4: 385-93
27. Mernagh TP, Cooney RP, Johnson RA. Raman spectra of Graphon carbon black. Carbon 1984; 22: 39-42
28. Kinoshita K, Carbon: Electrochemical and Physicochemical properties, John Wiley & Sons; Berkeley, California, USA: 1988
29. Endo M, Kim YJ, Maeda T, Koshiba K, and Katayama K. Morphological effect of the electrochemical behavior of electric double layer capacitors. J Mater. Res. 2001; 16: 3402-3410
30. Qu D and Shi H. Studies of activated carbons used in double-layer capacitors. J Power Sources 1998; 74: 99-107

**Table caption**

Table 1. Fundamental BET properties of MWNTs as a function of KOH addition are summarized.

**Figure captions**

Figure 1. The overall morphology of as-grown MWNTS (VGCF<sup>®</sup> and VGNF<sup>®</sup>) using FE-SEM (a, b) and the highly magnified structure of an individual fiber using HR-TEM (c, d).

Figure 2. High resolution nitrogen adsorption-desorption isotherms of mass-produced MWNTS activated at 800 °C for 1 hour using KOH/MWNTs ratios of 1 to 5 weight %, where the blank symbols indicate the adsorption results and the gray symbols imply results from the desorption.

○ indicates the result obtained from the pristine as-grown fiber, and □ to ○ indicate the activated MWNTs with additional KOH in the range of 100 to 500 wt. % of KOH addition.

Figure 3. Meso-pore size distribution profile using the BJH (Barrett-Joyner-Halenda) method of nitrogen gas desorption. ○ indicates the result obtained from the pristine as-grown fiber, and □ to ○ indicate the activated MWNTs with additional KOH in the range of 100 to 500 wt. % of

KOH addition.

Figure 4. Morphological variations after KOH activation using FE-SEM and HR-TEM with the magnification of 10,000 $\times$  and 250,000 $\times$ . Figures represent the MWNTs activated with KOH of (a) 100 wt. %, (b) 300 wt. % and (c) 500 wt. %. TEM photographs from (d) to (f) also show the fine surface structure in the same order.

Figure 5. Room temperature first-order and second-order Raman spectra of chemically activated MWNTs.

Figure 6. Relative intensity (R) variations of the Raman line and the in-plane crystallite size ( $L_a$ ) as a function of KOH addition.

Figure 7. Cyclic-voltammograms (CVs) of the MWNTS with a sweep rate of 1mV/s at various KOH addition ratios. Indication of      denotes as-grown fibers, and      to      indicate the MWNTs activated with KOH in the range of 100 to 500 wt. % KOH addition.

Figure 8. Variations of the specific capacitance per unit weight (F/g) obtained from the

KOH-activated MWNTs. The resultant capacitances are distinguished by their charging voltage; (a) capacitance uptake when charged to 2.5 V, and (b) charged to 3.5 V. Open symbols imply the results obtained at a 1 mA/cm<sup>2</sup> current density on discharge and gray symbols imply the results obtained at a 10mA/cm<sup>2</sup> current density on discharge.

Figure 9. Variation of the specific capacitance per unit area ( $\mu\text{F}/\text{cm}^2$ ) as a function of KOH addition. The resultant capacitances are distinguished by their charging voltage; (a) capacitance uptake when charged to 2.5 V and (b) when charged to 3.5 V. Open symbols imply the results obtained at a 1 mA/cm<sup>2</sup> current density on discharge and gray symbols imply the results obtained at a 10mA/cm<sup>2</sup> current density on discharge.